Electronic Supplementary Information

A low-cost and large-area modular nickel electrode on aramid fabric for efficient solar-driven water electrolysis

Yuling Yuan,[a] *Zhiping Mao,*[a,d] *Hong Xu,**[,a] *Fatwa F. Abdi,**[,b,c] *and Yimeng Ma**[,a,d]

[a.] Key Laboratory of Science and Technology of Eco-Textile, Ministry of Education; College of Chemistry and Chemical Engineering, Donghua University, Shanghai, 201620, China. E-mail: yimeng.ma@dhu.edu.cn; hxu@dhu.edu.cn

[b.] School of Energy and Environment, City University of Hong Kong, 83 Tat Chee Avenue, Kowloon, Hong Kong SAR, China. E-mail: ffabdi@cityu.edu.hk

[c.] Institute for Solar Fuels, Helmholtz-Zentrum Berlin für Materialien und Energie GmbH, Hahn-Meitner-Platz 1, Berlin, 14109, Germany.

[d.] National Innovation Center of Advanced Dyeing & Finishing Technology, Shandong Zhongkang Guochuang Research Institute of Advanced Dyeing & Finishing Technology Co., Ltd., Taian City, Shandong Province 271000, China.

1 Experimental Section

1.1 Materials

Aramid fabric (white, twill weave fabric, 200 g/m^2) was purchased from Shanghai Macy Industries Co., Ltd. 316 stainless-steel wire with diameter of 1 mm was purchased from Xinghua Hongxiang Stainless-steel Products Factory. Electromagnetic shielding cloth (Feillemei) were purchased from Yancheng Inheritance Clothing Trading Co., Ltd. Sodium hydroxide (NaOH; 98%), sulfuric acid (H_2SO_4; 98%), thioacetamide (C_2H_5NS; AR), nickel (II) sulfate hexahydrate ($NiSO_4·6H_2O$; GR, 99%), nickel chloride hexahydrate ($NiCl_2·6H_2O$; AR, 99%), and boric acid (H_3BO_3; 99.9% metals basis) were purchased from Sino Pharm Group Chemical Reagent Co., Ltd. Isopropyl alcohol (C_3H_8O; ≥ 99.7%), tin tetrachloride($SnCl_4$; ≥ 99%), iron sulfate heptahydrate ($FeSO_4·7H_2O$; ≥99.0%) and zinc power (Zn; AR, 200 mesh) was purchased from Shanghai Titan Technology Co., Ltd. Glycine ($C_2H_5NO_2$; AR, 99.5-100.5%) was purchased from Shanghai Wokai Chemical Reagent Co., Ltd. All the chemicals were used as received without any purification, and all the aqueous solutions were prepared with deionized (DI) water (18.25 MΩ cm, YL400BU, Yiliyuan).

1.2 Fabrication of Electrodes

1.2.1 Synthesis of SnS_2/Aramid

A piece of aramid cloth, according to specific requirement of size (4 × 8 cm^2), was firstly modified by sewing 316 stainless-steel wire (GS2700, Brother) with 1 cm spacing. The aramid cloth was sonicated at 80 ℃ for 3 hours in 1 M NaOH solution. Then, the aramid was rinsed with deionized (DI) water and dried in air at 60 ℃ for 3 hours. SnS_2 was synthesized on the aramid cloth according to a solvent-thermal method reported by Li *et al.*,[1] with a modification of the reactant concentration. Briefly, thioacetamide (0.2 g) was dissolved in isopropanol (30 mL). Then $SnCl_4$ (84 μL) was added to the isopropanol mixture and stirred to form a homogeneous solution before being transferred into a Teflon-lined stainless-steel autoclave. The stainless-steel/aramid cloth was placed standing against the wall of the autoclave, and heated at 180 °C for 24 h. After the reaction was completed and cooled to room temperature, the cloth was rinsed with DI water for at least 5 times and then sonicated in DI water for 3 minutes. The small-area SnS_2/aramid (1 × 1.5 cm^2) was

fabricated using the same above-mentioned method without the stainless-steel wire sewing.

1.2.2 Electrochemical Deposition of Ni on SnS_2/Aramid

The electrochemical deposition was modified according to a previous method reported by Ahmet *et al*.[2] Briefly, 0.5 M $FeSO_4 \cdot 7H_2O$, 1 M glycine were dissolved in DI water, and then the pH was adjusted to ~2.5 by adding H_2SO_4 or NaOH solution. Subsequently, 0.5 g of zinc powder was added to the solution, and the SnS_2/aramid cloth was immersed for 10 minutes. Finally, the treated SnS_2/aramid cloth was sonicated in DI water for 3 minutes.

The electrodeposition of Ni was carried out using a CHI 1140C potentiostat (CH Instruments) in a three-electrode configuration, using treated SnS_2/aramid as the working electrode (WE), platinum mesh electrode (2 × 2 cm^2) as the counter electrode (CE), and Ag/AgCl (3 M KCl) as the reference electrode (RE). The electrochemical bath contained 1.14 M $NiSO_4 \cdot 6H_2O$, 0.16 M $NiCl_2 \cdot 6H_2O$, and 0.73 M H_3BO_3 in 80mL DI water under magnetic stirring at 50 °C. A constant potential of -0.9 V versus Ag/AgCl was applied with magnetic stirring at 50 °C for 900 s (for 1 cm^2 substrates) or 1200 s (for 10-18 cm^2 substrates), followed by applying a current density of -10 mA cm^{-2} for 900 s. The resulted Ni/SnS_2/aramid was then sonicated in DI water for 3 minutes, and dried in air at 60 ℃ for 3 hours.

1.3 Characterization

1.3.1 Physical Characterization

The characterization of morphology and chemical composition of Ni/SnS_2/aramid, SnS_2/aramid and aramid was carried out on Hitachi S-4800 field-emission scanning electron microscope (SEM) at an accelerating voltage of 10 kV. The X-ray diffraction (XRD) data was acquired from a Haoyuan DX-2700BH X-ray diffractometer at a tube voltage of 40 kV with Cu Kα radiation (λ = 1.54184 Å). X-ray photoelectron spectroscopy (XPS) measurements were carried out using an Escalab 250 X-ray photoelectron spectrometer using Mg Kα as the excitation source to characterize the oxidation states and chemical bonding between the elements. The XPS data were corrected based on the C 1s peak at 284.8 eV. The inductively coupled plasma atomic

emission spectrometry (ICP-AES, Leeman Prodigy, USA) was applied to measure the content of elements in the 1 M NaOH electrolyte after 16-hour oxygen evolution reaction on Ni/SnS_2/aramid electrode. It is noted that transmission electron microscopy of our samples would be interesting but the presence of strongly magnetic metallic nickel complicated its measurement due to the potential damage to our equipment. The thermogravimetric analysis (TGA) was carried out using a thermogravimetric analyzer (Netzsch TG209 F1 Libra) to determine the thermal stability of the unmodified aramid fabric between 50–800 ℃at a heating rate of 10 ℃/min under N_2 atmosphere.

1.3.2 Electrochemical Characterization

Cyclic voltammetry (CV) and linear sweep voltammetry (LSV) were carried out in a 1 M NaOH electrolyte (pH 13.8) at room temperature in a three-, or two-, electrode configuration where indicated. In the two-electrode configuration, Pt mesh or Ni/SnS_2/aramid was used as the counter electrode where specified. In the three-electrode configuration, the applied potentials versus Ag/AgCl were converted to the potentials versus reversible hydrogen electrode (RHE) by the Nernst equation:

$$E_{RHE} = 0.0591 * pH + E^0_{Ag/AgCl} + E_{Ag/AgCl} \quad \text{Equation S1}$$

where E_{RHE} is the applied potential versus RHE; $E^0_{Ag/AgCl}$ is the standard potential of the Ag/AgCl reference electrode (0.198 V_{RHE} at 25 °C) and $E_{Ag/AgCl}$ is the applied potential versus Ag/AgCl.

Prior to the electrochemical measurements, Ni/SnS_2/aramid electrodes were conditioned using the CV at 100 mV s^{-1} until stabilized between 0.9~2.2 V_{RHE} for OER, 0~-0.8 V_{RHE} for HER in a three-electrode configuration, and 1~2.5 V versus Ni for OER, -1.5~-3 V versus Ni for HER in a two-electrode configuration, respectively. The scan rate of the CV measurements was 1 mV s^{-1}. The steady-state current measured for each electrode was recorded at 100 s in a chronoamperometric measurement at the specified applied potential.

The quantification of H_2 and O_2 evolution using Ni/SnS_2/aramid electrodes was carried out using a gas-tight circulation and collection system (Labsolar-6A, Beijing Perfectlight) during the electrochemical measurement. The applied potential was set at

1.8 V versus Ni using an Autolab potentiostat (PGSTAT 204, Metrohm) and Nova 1.11 software in a two-electrode configuration where both working and counter electrodes were the Ni/SnS_2/aramid (1 cm^2). H_2 and O_2 were generated in the circulation system and then were sent automatically to a gas chromatography (GC, GC9790II, FuLi Instruments) at the time interval of 0.5 h. The gas circulation system was initially vacuumed to 1 kPa. Then H_2 and O_2 were continuously generated to build up the gas pressure in the system. The total volume of the system is approximately 600 mL and the sampling volume is 0.6 mL. The H_2 and O_2 mixture was injected into a RubyBond^{TM} 5A column in the GC by argon gas carrier at 373 K and both products were detected in a thermal conductivity detector (TCD) at 423 K. H_2 and O_2 calibration was carried out using 99.999% H_2 generated by an alkaline electrolyzer (SPH-300, Beijing BCHP) and 99.999% O_2 (Air Liquide). The Faraday efficiency (FE) of OER and HER ($4OH^- - 4e^- \rightarrow O_2 + 2H_2O$; $2H_2O + 2e^- \rightarrow H_2 + 2OH^-$) was calculated according to the following equation:

$$FE = \frac{charges\ for\ evolution}{total\ charges\ charges\ generated} = \frac{n \times z \times F}{I \times t} \times 100\% \qquad \text{Equation S2}$$

where n (mol) is the number of moles of oxygen or hydrogen generated; I (A) is the current generated during the measurement time (t, seconds) biases at 1.8 V versus Ni; z is the number of electrons involved in the OER (z = 4) and HER (z = 2); F (C mol^{-1}) is the Faraday constant (96 485 C mol^{-1}).

1.3.3 Determination of the Effective Surface Area of the Ni/SnS_2/Aramid Electrode

The roughness factor of the Ni/SnS_2/aramid electrode was calculated considering our previous microkinetic analyses of Ni/FTO electrode.[3] Assuming no mass transport limitation occurred in both small area (1 cm^2) Ni/SnS_2/aramid and Ni/FTO electrodes, the OER currents measured in both electrodes were simply proportional to the density of catalytic species (NiOOH(4+)). Therefore, the current is then proportional to the surface area.

In our previous study of Ni/FTO, we take the catalytic current at 1.6 V_{RHE}, giving an OER current density of 4 mA cm^{-2} (active surface area). In the Ni/SnS_2/aramid electrode, the OER current was measured to be 20 mA cm^{-2} (geometric area) shown in Figure 3a. Therefore, the proportion between these two electrodes current density is the effective roughness factor, which is determined to be 5.

1.3.4 Solar-Driven Water Splitting Characterization

A stand-alone PV-EC device consists of a polycrystalline Si PV device (3 × 2.5 cm^2, Tengxia Optoelectronics) and two 10 cm^2 Ni/SnS_2/aramid electrodes in a 1 M NaOH electrolyte. The current-voltage (IV) curve of the PV was carried out using the CHI 1440C potentiostat and the LSV measurement was carried out at 100 mV s^{-1}. A 300 W Xe lamp with an AM 1.5G filter (Microsolar 300, Beijing Perfectlight) was employed to simulate the solar irradiation. The intensity was calibrated using a calibrated Si photodiode (FDS1010-CAL, Thorlabs) between 300 nm and 1100 nm to be 1 sun equivalent. The stability measurement was carried out by connecting these two Ni/SnS_2/aramid electrodes to the Si PV and CHI 1440C was connected in series with the circuit on the chronoamperometric mode with 0 V potential applied. The measurement was conducted for over 5 days (> 120 hours) under the continuous simulated AM 1.5G irradiation.

The solar-to-hydrogen conversion efficiency (STH%) was calculated using the following equation:

$$STH\% = \frac{Chemical\ energy\ output}{Solar\ energy\ input} \times 100\% = \frac{j_{op} \times A \times E_f \times FE_{H_2}}{P_S \times A} \times 100\% \qquad \text{Equation S3}$$

where j_{op} (mA cm^{-2}) is the operating current density of the combined system; A (cm^2) is the effective illuminated area (7.5 cm^2 in this work); E_f (V) is the standard thermodynamic potential difference between hydrogen evolution and oxygen evolution half-reactions (1.23 V) that is corresponded to the change of Gibbs free energy of overall water splitting; FE_{H_2} is the Faraday efficiency for hydrogen evolution that is measured to be 100 % in this study and P_S (mW cm^{-2}) is the power of the AM 1.5G solar illumination (100 mW cm^{-2}).

1.4 Electrochemical Simulations

The schematic cell geometry considered in our electrochemical simulations are shown in Scheme S1. A 2-D channel electrochemical flow cell with channel width w_{cell} and cell height h_{cell} was simulated. The electrodes are located at the centre of the channel side walls, and the height of the electrode h_{el} were varied in the simulations. The baseline parameters used in our simulations are listed in Table S1, and steady state simulations

were performed with COMSOL Multiphysics® 6.0 using PARDISO general solver to solve the governing conservation and transport equations (see below). Relative tolerance of 10^{-4} was applied as the convergence criterion.

Since the Reynolds number (*Re*) calculated using our cell configuration is very low, laminar flow is assumed in the electrochemical cell. The electrolyte velocity vector (u) in the electrochemical cell was determined by solving the mass and momentum conservation equations (Navier-Stokes equation) under laminar flow condition.

$$\rho \nabla . u = 0 \qquad \text{Equation S4}$$

$$\rho u . \nabla u = -\nabla p + \mu \nabla^2 u + \rho g \qquad \text{Equation S5}$$

ρ is the density, p is the pressure, μ is the viscosity and g is gravity. The solution provided a parabolic velocity profile in the electrochemical cell. The boundary conditions consisted of an inlet velocity v_{in} normal to the inlet with fully developed flow. The pressure at the outlet is set to 1 bar. No-slip boundary conditions were used at the walls of the cell.

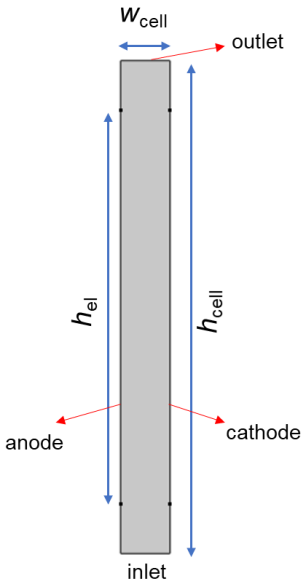

Scheme S1. Schematic of the computational domain consisting of the liquid electrolytes (with inlet and outlet) and two electrodes. h_{cell} = cell height, w_{cell} = cell width, h_{el} = electrode height.

Theory of diluted species was used to solve the mass-transport processes of dissolved ions.

$$\frac{dc_i}{dt} = -\nabla \cdot \boldsymbol{N}_i = -\nabla \cdot \left(-D_i \nabla c_i - \frac{Z_i F}{RT} D_i c_i \nabla \phi_l + c_i u\right) \qquad \text{Equation S6}$$

where c_i, N_i, D_i, and Z_i are the concentration, the molar flux, the diffusion coefficient, and the charge of dissolved species, i, respectively. ϕ_l is the electrolyte potential, F is the Faraday constant, R is the gas constant, and T is temperature. We assumed charge neutrality and charge conservation in the electrolyte solution.

$$\sum Z_i c_i = 0 \qquad \text{Equation S7}$$

$$\nabla \cdot \boldsymbol{j}_l = \nabla \cdot (F \sum Z_i \boldsymbol{N}_i) = 0 \qquad \text{Equation S8}$$

j_l is the electrolyte current density. In the present study, the electrolyte is 1 M NaOH, which was used as the initial concentration ($c_{i,0}$) of Na^+ and OH^- throughout the electrolyte. At the inlet, constant concentration boundary condition ($c_i = c_{i,0}$) was used.

The electrode current density at the electrode surface, j_s, is set to be equal to the electrolyte current density normal to the surface.

$$\boldsymbol{n} \cdot \boldsymbol{j}_l = j_s \qquad \text{Equation S9}$$

$\boldsymbol{n}$ is the normal vector to the electrode boundary. Since the electrolyte used in our study is highly alkaline, hydroxyl ions (OH^-) are assumed to be the reactant on the anode as well as the product on the cathode. The local current density at the electrodes then defines the molar flux of ions at the electrode surface.

$$\boldsymbol{n} \cdot \boldsymbol{N}_i = \frac{-\nu_i j_s}{n_e F} \qquad \text{Equation S10}$$

ν_i is the stoichiometry coefficient for species i, and n_e is the number of electrons involved in the reaction. For OH^-, the values for ν_i and n_e are both 4 for the OER and 2 for the HER. The normal molar flux for the other dissolved species at the electrode surface (i.e., Na^+) is zero.

The local current density was determined by Butler-Volmer equation considering mass action law dependent exchange current density.

$$j_s = j_0 \left(\prod_{i:\nu_i>0} \left(\frac{c_i}{c_{i,0}}\right)^{\nu_i} exp\left(\frac{\alpha_a F \eta}{RT}\right) - \prod_{i:\nu_i<0} \left(\frac{c_i}{c_{i,0}}\right)^{-\nu_i} exp\left(\frac{\alpha_c F \eta}{RT}\right) \right) \qquad \text{Equation S11}$$

$$\eta = \phi_s - \phi_l - E_{\text{eq}} - \frac{RT}{n_e F} ln \prod_i \left(\frac{c_i}{c_{i,0}}\right)^{\nu_i} \qquad \text{Equation S12}$$

where j_0 is the exchange current density, α_a is the anodic transfer coefficient, α_c is the cathodic transfer coefficient, η is the overpotential, ϕ_s is the electric potential at the

electrode, and E_{eq} is the equilibrium potential for the reaction. At the anode, the average current density (j_{app}) is set, and the cathode potential is set to be 0 V.

2 Supplementary Tables

Table S1. Table of baseline parameters used in the simulations. Unless specifically mentioned in the manuscript text or figure captions, the parameters here were used.

	Parameter	Value	Ref.
Electrolyte	Initial Na^+ concentration, $c_{Na^+,0}$	1 M	
	Initial OH^- concentration, $c_{OH^-,0}$	1 M	
	Diffusivity of H^+, D_{OH^-}	5.3×10^{-9} m^2/s	Ref [4]
	Diffusivity of Na^+, D_{Na^+}	1.33×10^{-9} m^2/s	Ref [4]
	Inlet velocity, v_{in}	10^{-6} m/s	
	Outlet pressure, p_{out}	10^5 Pa	
	Dynamic viscosity, μ	1.01 mPa s	
	Density, ρ	998.2 kg/m^3	
	Temperature	293.15 K	
Electrode	Equilibrium potential for HER, $E_{eq,HER}$	0 V	
	Equilibrium potential for OER, $E_{eq,OER}$	1.23 V	
	HER exchange current density, $j_{0,HER}$	10 A/m^2	
	HER anodic transfer coefficient, $\alpha_{a,HER}$	0.5	
	OER exchange current density, $i_{0,OER}$	10^{-2} A/m^2	
	OER anodic transfer coefficient, $\alpha_{a,OER}$	0.7	
	Cathodic transfer coefficient, α_c	n_e - α_a	
	Applied average current density, j_{app}	up to 20 mA/cm^2	
Geometry	Cell height, h_{cell}	10 cm	
	Cell width, w_{cell}	1 cm	
	Electrode height, h_{el}	1 – 9 cm	

Table S2. The ICP-AES results of the elements in 1 M NaOH electrolyte after 16 hours water splitting for both oxygen and hydrogen evolutions on two Ni/SnS_2/aramid electrodes.

Elements	**Ni**	**Sn**	**S**	**Fe**	**Cr**
Concentration / ppm	≤ 0.01	5.08	1.97	0.12	≤ 0.01

3 Supplementary Figures

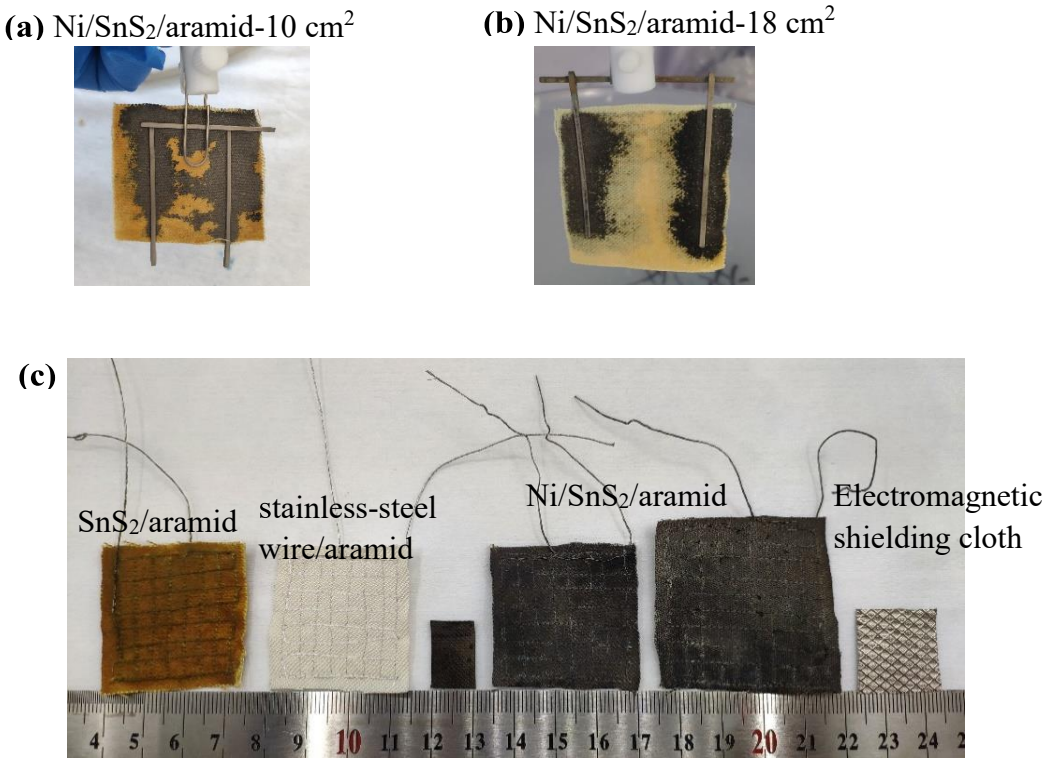

Figure S1. Optical photos of (a) Ni/SnS_2/aramid-10 cm^2 and (b)18 cm^2 with the uncoated patches, and (c) from left to right are the SnS_2/aramid-10 cm^2, stainless-steel wire/aramid-10 cm^2, Ni/SnS_2/aramid-1 × 1.5 cm^2, Ni/SnS_2/aramid-10 cm^2, Ni/SnS_2/aramid-18 cm^2 and electromagnetic shielding cloth-4 cm^2.

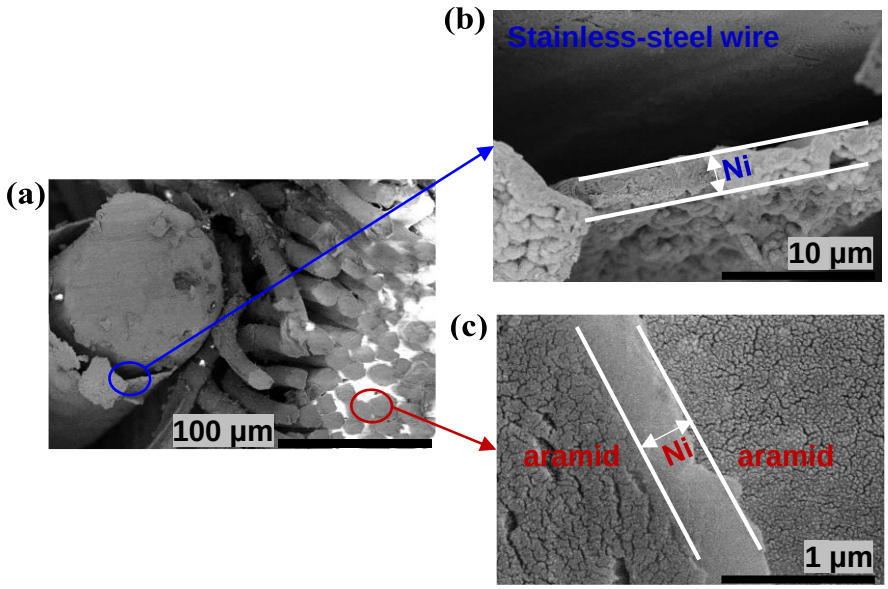

Figure S2. SEM images of the cross section of (a) Ni/SnS_2/aramid with stainless-steel wire, and the corresponding local magnification images for (b) stainless-steel wire (blue circle) and (c) Ni/SnS_2/aramid (red circle).

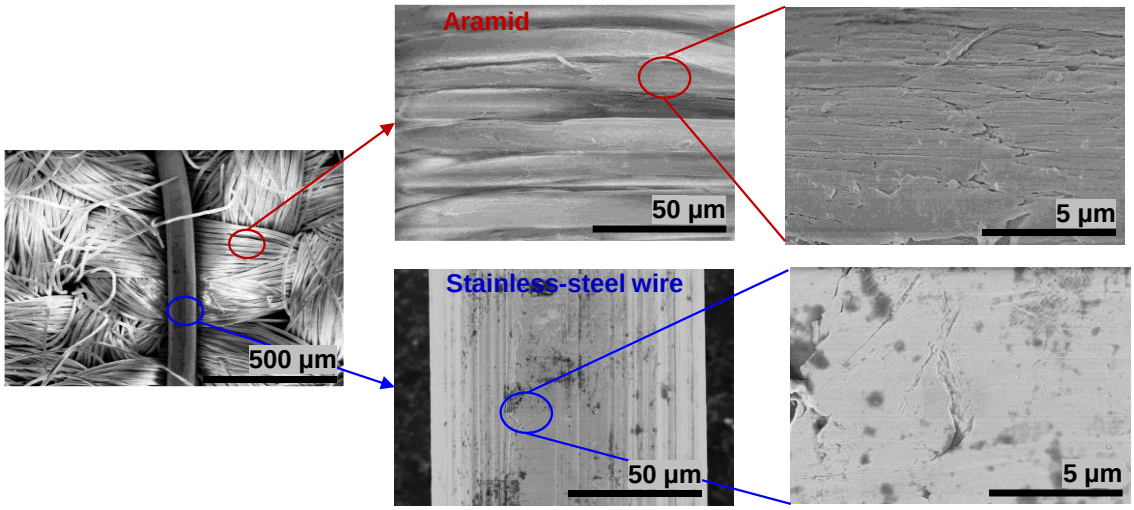

Figure S3. SEM images of aramid with stainless-steel wire.

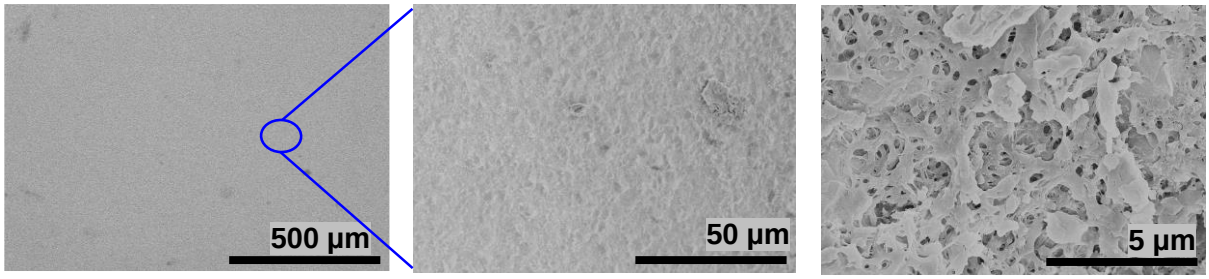

Figure S4. SEM images of Ni/FTO.

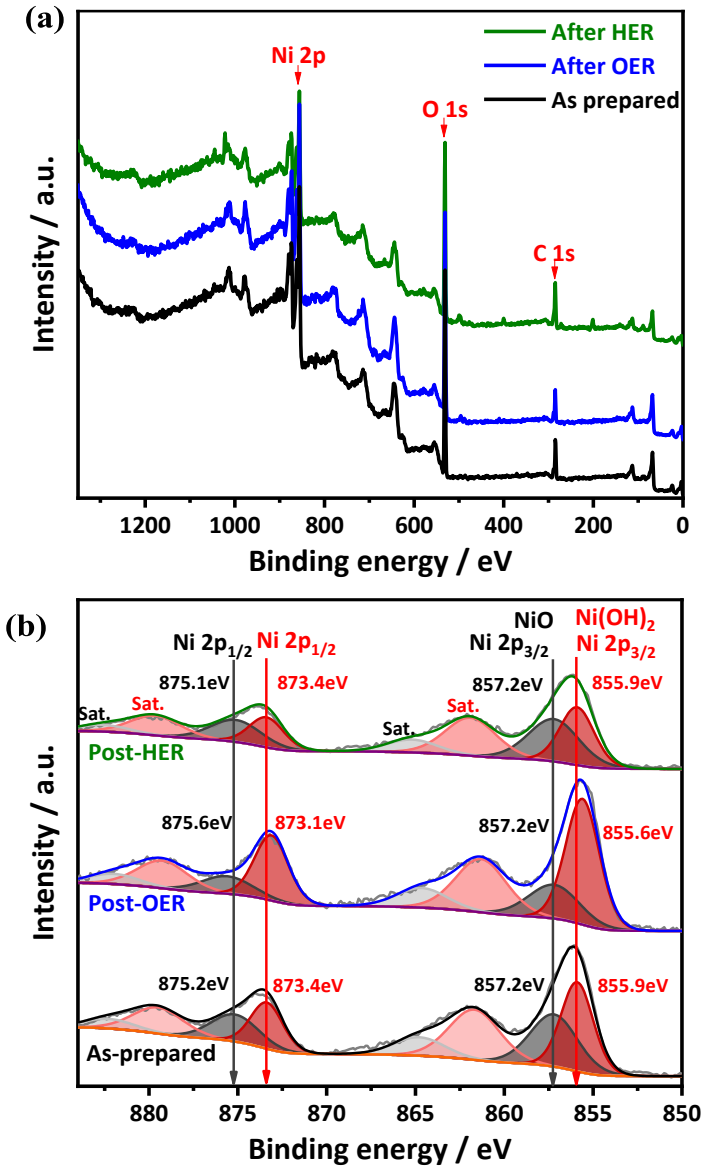

Figure S5. XPS data of Ni/SnS_2/aramid as prepared, post-HER and post-OER (after 10 hours OER or HER testing). (a) overview and (b) deconvolution of Ni 2p peaks to determine the NiO and $Ni(OH)_2$.

(a) Post-OER

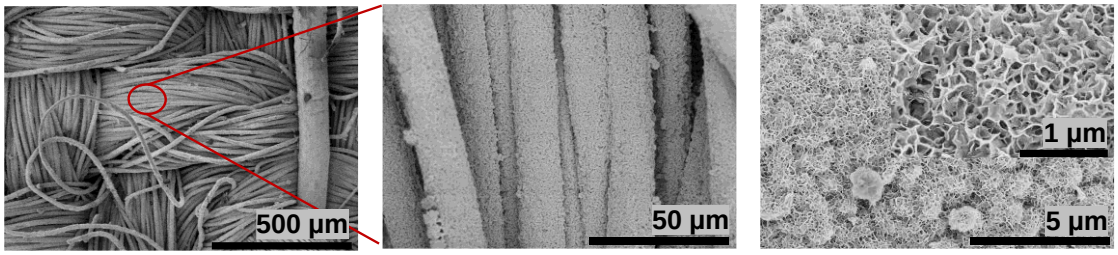

(b) Post-HER

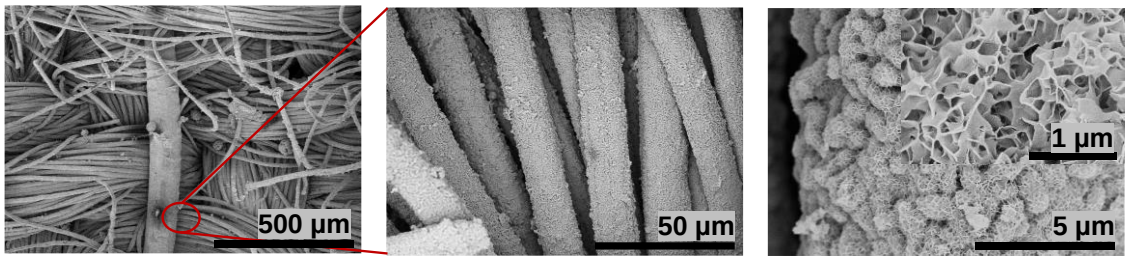

Figure S6. SEM images of Ni/SnS_2/aramid electrodes (a) post-OER and (b) post-HER (after 10 hours HER or HER testing).

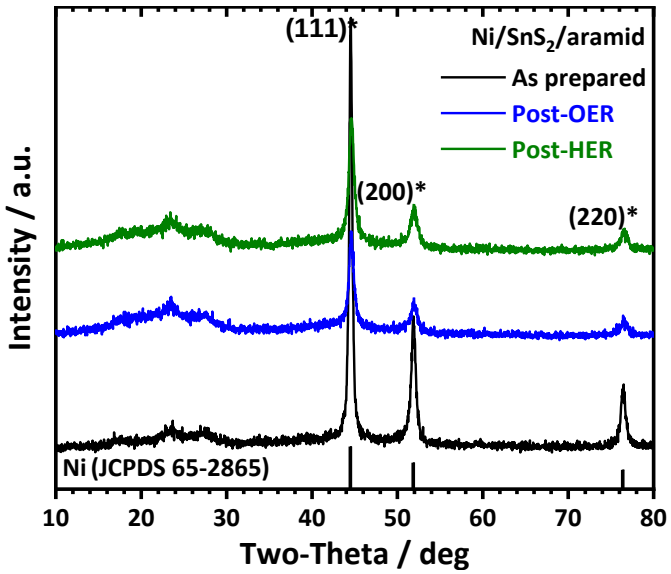

Figure S7. XRD data of Ni/SnS_2/aramid as-prepared (black, JCPDS:65-22856), post-OER (blue) and post-HER (green), respectively.

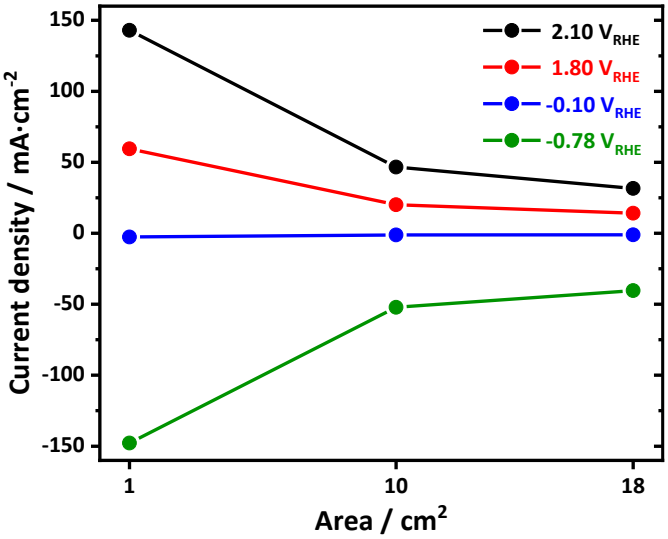

Figure S8. The steady-state current density of Ni/SnS_2/aramid electrodes under different applied potential as a function of electrode area based on the three-electrode configuration. Black: 2.1 V_{RHE}. Red: 1.8V_{RHE}. Blue: -0.1 V_{RHE}. Green: -0.78 V_{RHE}.

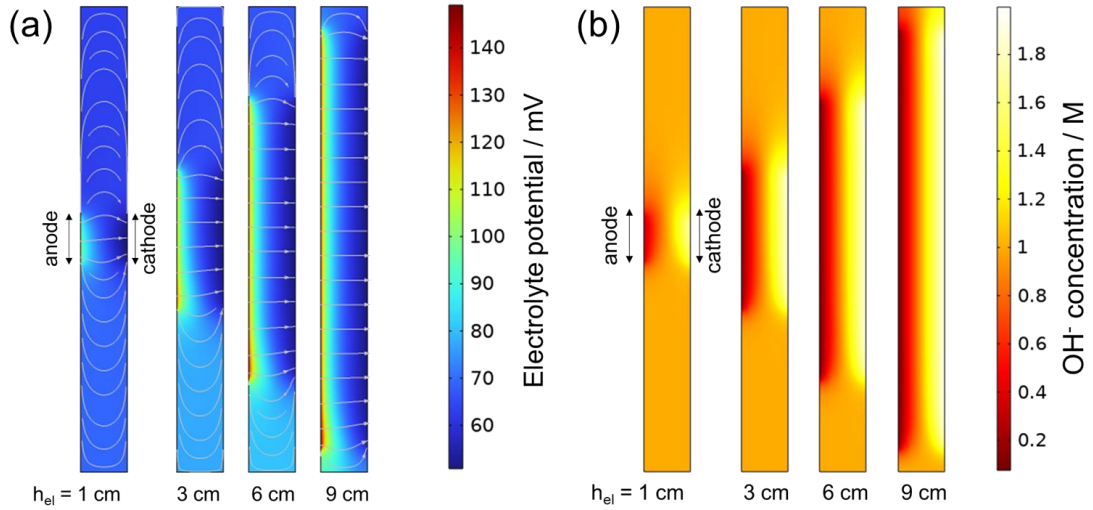

Figure S9. Colormaps of (a) electrolyte potential and (b) hydroxide (OH^-) concentration as simulated using the 2D multiphysics model for the electrochemical cell with electrodes of increasing size (h_{el}) from 1 to 9 cm at the current density of 20 mA cm^{-2}. Arrows in (a) depict the current density vectors.

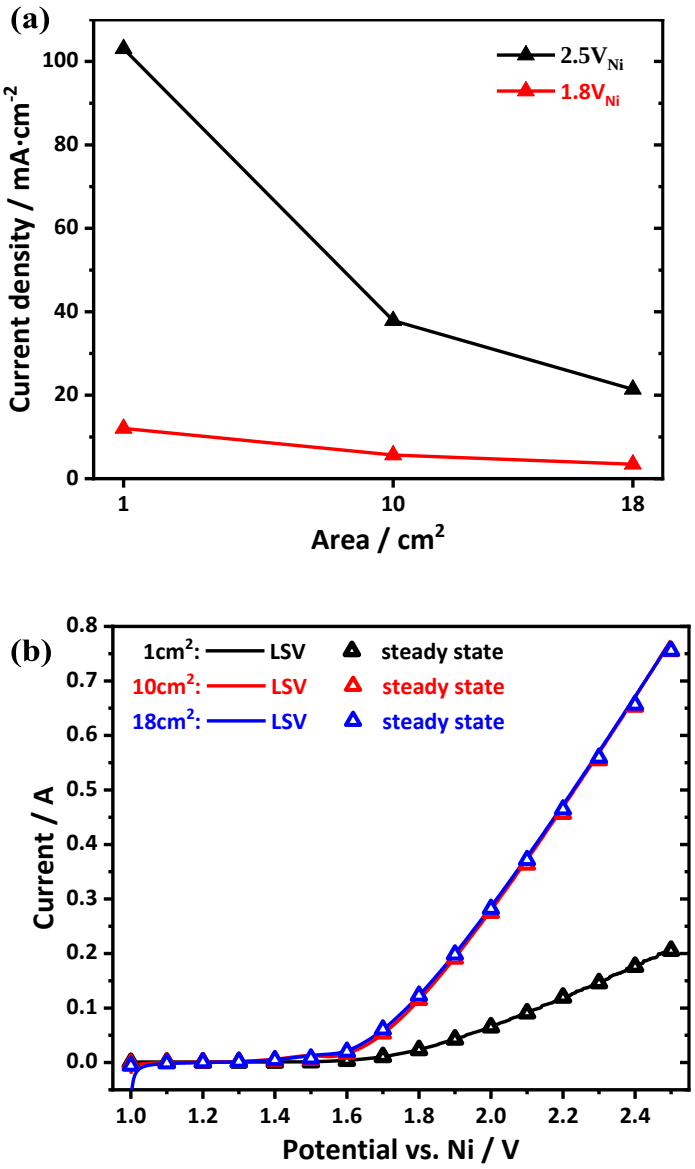

Figure S10. (a) The steady-state current density of Ni/SnS_2/aramid electrodes under different applied potential as a function of electrode area. Black: 2.5 V versus Ni. Red: 1.8 V versus Ni. (b) LSV curves versus current measured using the Ni/SnS_2/aramid as the working electrode and counter electrode in the two-electrode configuration with different electrode size: 1 cm^2 (black),10 cm^2 (red) and 18 cm^2 (blue) and the corresponding steady-state current (empty circles).

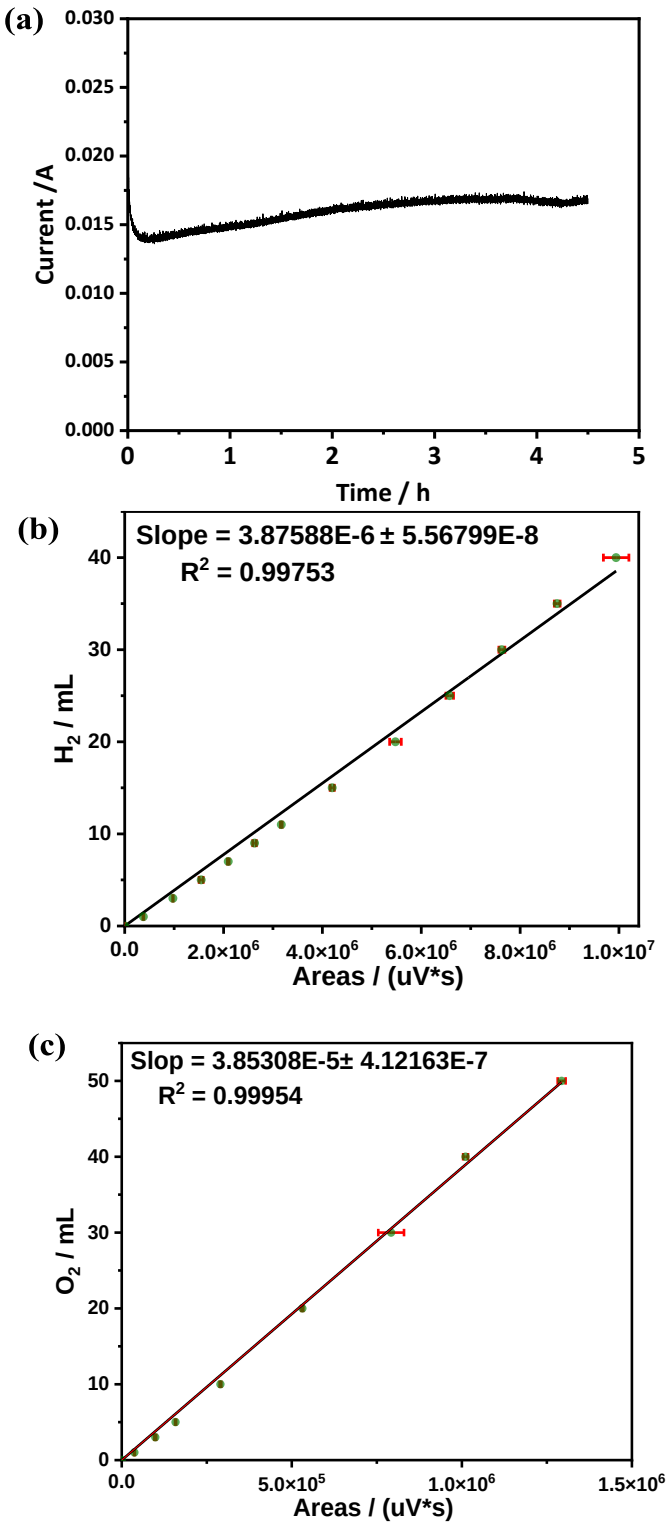
(a)
Current /A
Time / h
(b)
Slope = 3.87588E-6 ± 5.56799E-8
R2 = 0.99753
H2 / mL
Areas / (uV*s)
(c)
Slop = 3.85308E-5± 4.12163E-7
R2 = 0.99954
O2 / mL
Areas / (uV*s)

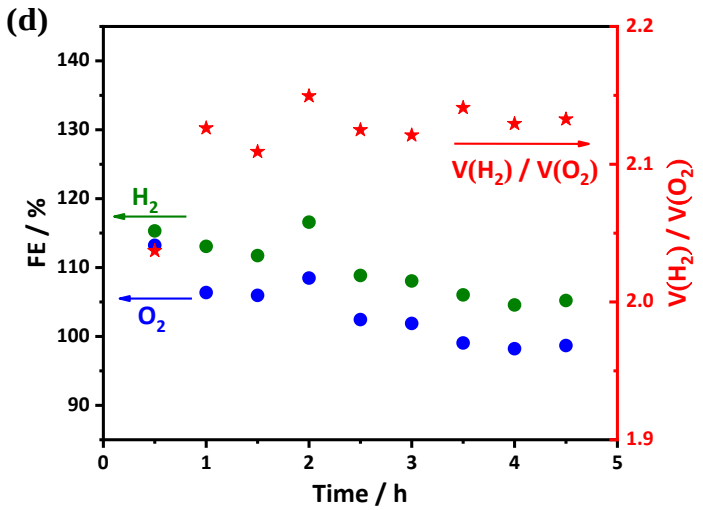

Figure S11. (a) Time dependence of the current under a constant potential of 1.8 V for Ni/SnS_2/aramid electrodes (1 cm^2) based on two-electrode configuration in 1 M NaOH. (b) and (c) The standard curve for the electrochemical production of H_2 and O_2 determined by gas chromatography. (d) The FE of H_2 (green circle) and O_2 (blue circle) and the corresponding volume ratio (red star) measured experimentally.

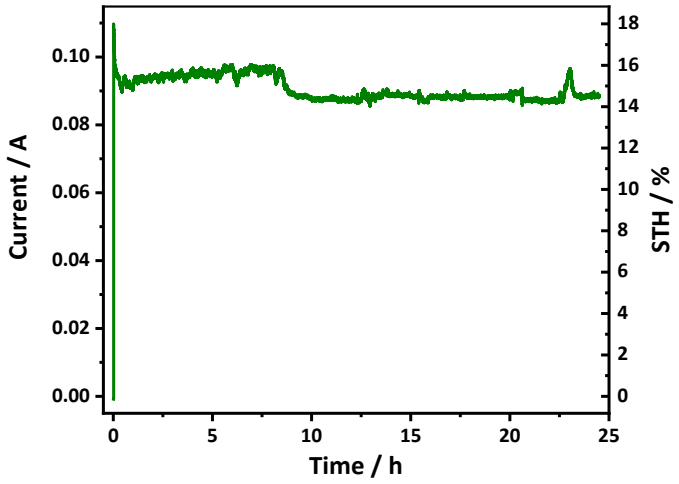

Figure S12. Current-time curve of the solar-driven water splitting device and the calculated STH conversion efficiency under simulated AM 1.5G illumination.

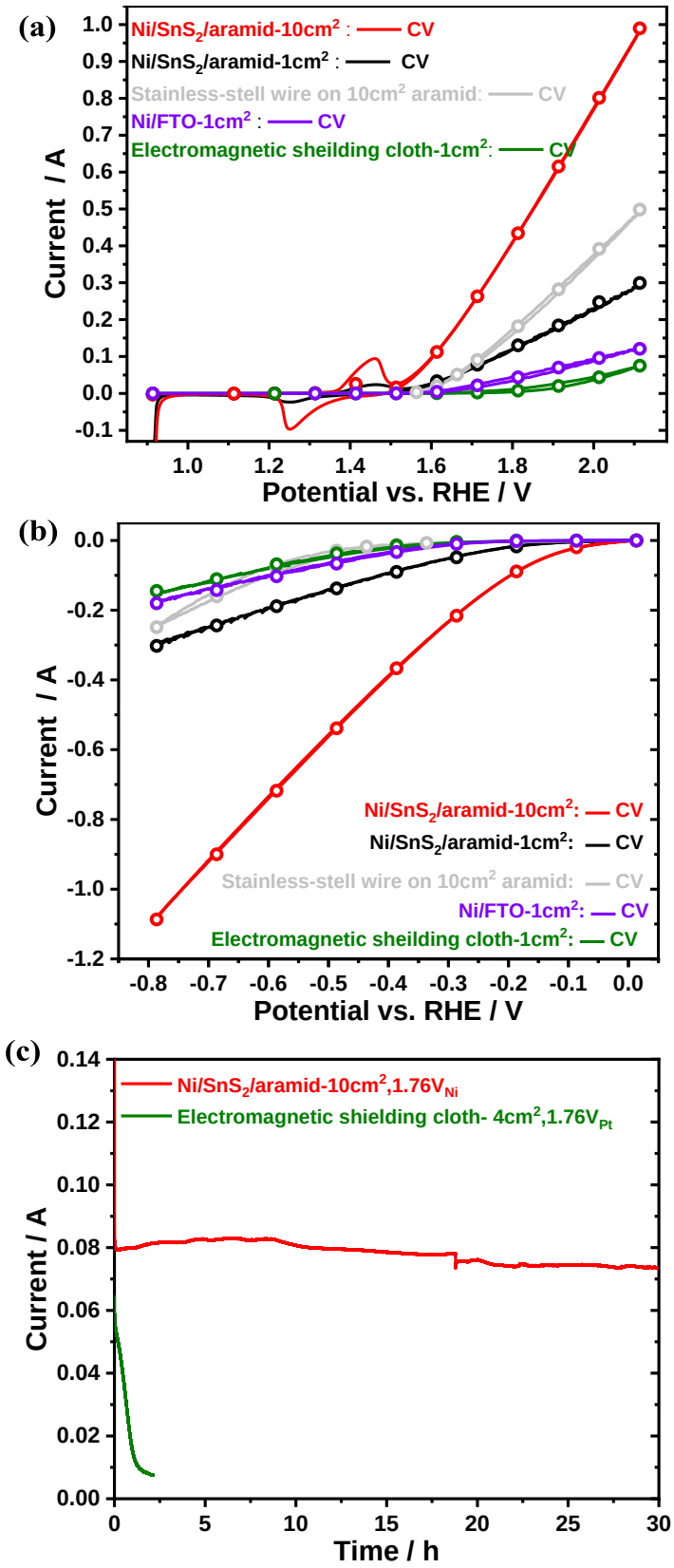

Figure S13. CV curves for (a) OER and (b) HER at 1 mV s^{-1} based on the three-electrode configuration in 1 M NaOH; empty circles represent the steady-state current measured at each specific potential. (c) Time dependence of the current under 1.76 V versus Ni for

Ni/SnS_2/aramid electrode (red) based on the two-electrode configuration and 1.76 V versus Pt for electromagnetic shielding cloth (green), based on a three-electrode configuration, respectively.

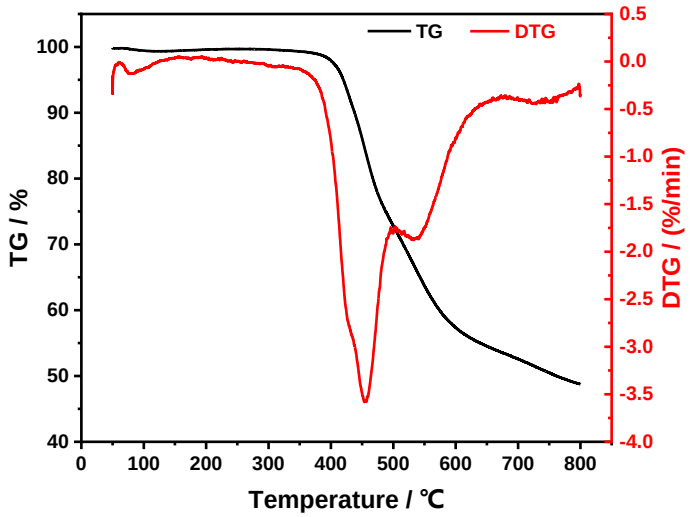

Figure S14. The thermalgravimetric analysis of aramid fabric without treatment. The residual mass of aramid fabric is 48.76% at 799.7℃.

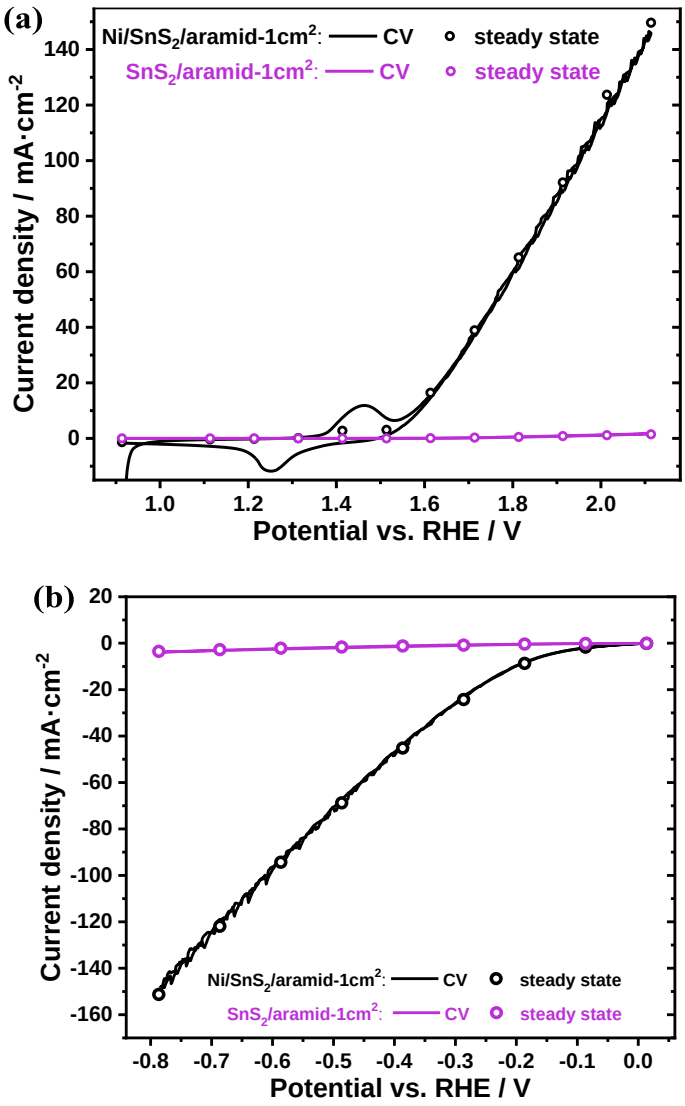

Figure S15. The comparation of CV curves for (a) OER and (b) HER on Ni/SnS_2/aramid-1 cm^2 and SnS_2/aramid-1 cm^2 based on the three-electrode configuration in 1 M NaOH; the scan rate of CV curves is 1 mV s^{-1}; empty circles represent the steady-state current measured at each specific potential.

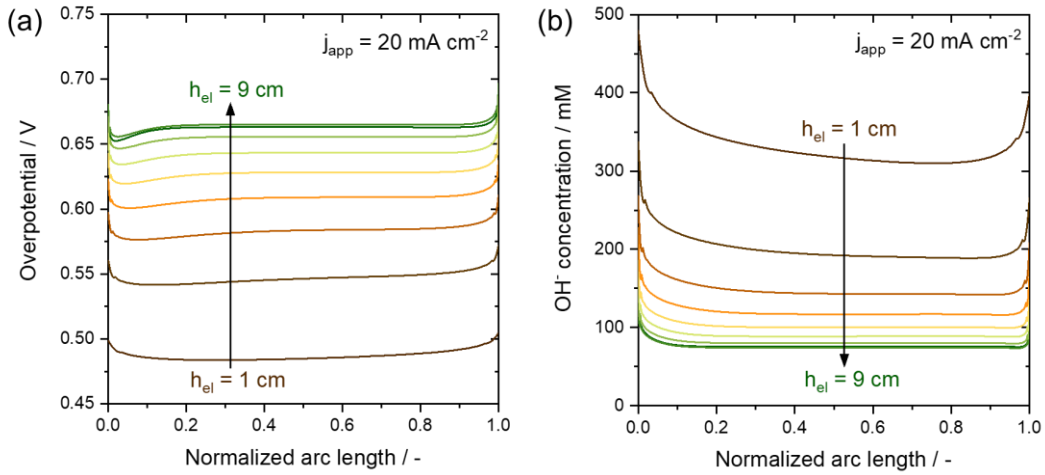

Figure S16. Local distribution of (a) overpotential and (b) hydroxide (OH^-) concentration at the surface of the anode as simulated using the 2D multiphysics model for the electrochemical cell with electrodes of increasing size (h_{el}) from 1 to 9 cm at the current density of 20 mA cm^{-2}.

References

1. F. Li, L. Chen, G. P. Knowles, D. R. MacFarlane and J. Zhang, *Angew. Chem. Int. Ed.*, 2017, **56**, 505-509.
2. I. Y. Ahmet, Y. Ma, J.-W. Jang, T. Henschel, B. Stannowski, T. Lopes, A. Vilanova, A. Mendes, F. F. Abdi and R. van de Krol, *Sustain. Energ. Fuels*, 2019, **3**, 2366-2379.
3. Y. Yuan, Y. Guo, W. Wu, Z. Mao, H. Xu and Y. Ma, *ACS Energy Lett.*, 2022, **7**, 3276-3285.
4. D. G. Leaist and B. Wiens, *Can. J. Chem.*, 1986, **64**, 1007-1011.